Article

Effect of SiO$_2$/Organosilicone Double Insulation Coating Processes on the Properties of Ferrosilicon Magnetic Cores

Shaochuan Lin, Zihan Zhou, Jinghan Jin *, Xueyan Hu, Shaogang Li and Nachaun Ju

Key Laboratory of Green Fabrication and Surface Technology of Advanced Metal Materials,
Anhui University of Technology, Ma'anshan 243002, China; chaim_lsc@163.com (S.L.)
* Correspondence: a2592482502@163.com; Tel.: +86-0555-231-1571

Abstract: A nano-SiO$_2$ inorganic insulation layer was coated on the surface of FeSi magnetic powder via in situ fluidised vapour deposition. The surface was then coated with organosilicon resin to form an inorganic/organic double-insulating layer. Post-forming and annealing, a ferrosilicon magnetic powder core was prepared. The effects of organosilicon resin content and pressing pressure on the permeability and loss of the ferrosilicon magnetic core were studied. When the ferrosilicon magnetic core was doubly insulated with SiO$_2$/silicone resin, the silicone resin content increased, the insulation coating gradually thickens, and the saturation magnetic-induction intensity of the magnet gradually decreases; the density and effective permeability showed a trend of increasing first and then decreasing. Increasing the forming pressure can reduce the loss of the core, thereby improving the performance of the core and increasing the permeability without damaging the double-cladding layer. In the powder with the optimised silicone resin content (1.5 wt.%), the magnetic properties of the magnetic core were maximised after preparation at 1500 MPa followed by heat treatment at 773 K. The saturation magnetisation was 187.5 emu/g and the resistivity and permeability reached 10.5 Ω·cm and 49.6, respectively, at 100 mT and 50 kHz. The total loss was 905 mW/cm^3.

Keywords: magnetic core; ferrosilicon alloy; double cladding; magnetic energy

1. Introduction

Owing to their good saturation magnetization, high permeability, and relatively low core loss in the high-frequency range, iron-based soft magnetic composites have become key components of commercial electromagnetic systems such as filters, transformers, and small electronics [1–5]. Coating the prepared magnetic cores with insulation is important for preventing direct contact with magnetic particles and reducing the eddy current loss. Insulation coating agents are broadly divided into organic and inorganic coating agents. The main organic coating agent is a thermosetting resin, which is mixed with a curing agent to ensure the strength of the magnetic core [6–13]. Further, inorganic coating agents are mainly mineral powders with high resistivity, silicate, phosphate, and various oxides such as phosphating layers, Al$_2$O$_3$, TiO$_2$, ZrO$_2$, and ferrite [14–21]. The phosphating process is now mature, yielding phosphate coatings with high resistivity and heat resistance, which will effectively reduce eddy current losses when applied to the magnetic core. Therefore, phosphate/silicone composite is a commonly used coating for magnetic cores. The magnetic core introduces a large internal stress during the pressing process, which is effectively reduced by an annealing treatment. Annealing also reduces hysteresis loss. However, the organic resin is prone to ageing or decomposition in the annealing process, which sharply degrades the insulation coating effect and consequently increases the eddy current loss [16]. In contrast, SiO$_2$ is a commonly used inorganic material with excellent insulation properties at high temperatures.

At present, nano-SiO$_2$ can be added in three ways: physical doping, chemical coating, or SO$_2$ deposition on the magnetic-powder surface. Physical doping is disadvantaged by

the difficulty of distributing SiO_2 evenly during the mixing process, resulting in poor uniformity and integrity of the insulation layer on the surface of the magnetic powder [22,23]. In the chemical coating method, a sol-gel is formed on the magnetic powder surface to generate the SiO_2 coating layer. This method is costly and requires optimisation and adjustment of the chemical solution and reaction conditions whenever the magnetic powder composition and particle size are changed [24–27]. In contrast, SiO_2 deposition through physical or chemical vapour deposition can be optimised to achieve a high quality of SiO_2 coating on the magnetic powder surface [13,28–31]. In previous studies, the author's research group demonstrated that adding fluidisation to the traditional vapour deposition process maintains the magnetic powder in a fluidisation suspension; moreover, the vapour-phase SiO_2 medium will nucleate and grow uniformly on the ferromagnetic powder surface. This technology synthesises soft magnetic composite powder that maintains the integrity of the core–shell structure. Moreover, the thickness of a non-magnetic SiO_2 insulation coating agent can be limited to the nanometre scale.

Inspired by the SiO_2 insulation coating on the surface of FeSi alloy powder, herein, an inorganic/organic (SiO_2/organosilicone resin) composite insulation layer is designed, and a ferrosilicon magnetic core with a SiO_2/organosilicone resin double coating is prepared. The effects of organosilicon resin content and pressing pressure on the permeability and loss of the ferrosilica–ferrosilicon magnetic core are studied in detail. The results provide a reference for further improving the efficiency of ferro-based magnetic cores in practical applications.

2. Experiment

2.1. Experimental Raw Materials

The raw material was Fe-6.5 wt.%Si alloy powder (99.9 wt.%; Platinum Advanced Material Co., Ltd., Guangdong, China) with a particle size of about 50μm. Ethyl orthosilicate ($Si(OC_2H_5)_4$; Kunshan Southeast Chemical Materials Co., Ltd., Jiangsu, China) was used as the precursor of the gaseous SiO_2 insulating medium and high purity Ar gas (>99.99 wt.%, Nanjing Special Gas Plant Co., Ltd., Jiangsu, China) was utilized as the carrier and dilution gas. The organic insulating agent and organic solvent were organic silicone resin (wacker-50, Wacker Chemical Reagent Co., Ltd., Germany) and acetone (Guangzhou Chemical Reagent Factory, China), respectively.

2.2. Preparation of the Ferrosilicon Magnetic Core

First, 50 g of Fe-6.5 wt.%Si powder was weighed and placed in a fluidised vapour deposition furnace independently developed by the research group. To convert the powder to the agglomeration fluidised state, Ar gas was injected as a diluent gas. When the temperature in the furnace rose to 953 K, 5 mL of liquid ethyl orthosilicate was pumped into the liquid evaporator for gasification at 423 K before entering the tubular furnace in an Ar gas flow (150 mL·min^{-1}). The whole reaction process was maintained at atmospheric pressure for 60 min. The furnace was then cooled to obtain Fe-6.5 wt.%)Si/SiO_2 composite powder. The obtained composite powder was added to an acetone resin solution (silicone resin to acetone mass ratio = 1:10; composite powder to acetone resin mass ratio = 100:1) in a water bath heated to 323 K. The mixture was electrically stirred to obtain a dry powder of ferrosilicon alloy doubly insulated with SiO_2 and organosilicone. Figure 1 is a schematic of the inorganic/organic double-layer coating.

Finally, approximately 6 g of the ferrosilicon alloy powder doubly coated with SiO_2/silicone resin was weighed and poured into the mould. After applying a four-column hydraulic press at 1500 MPa for 5 s, ring samples with an inner diameter, outer diameter, and heights of 14.4, 26.9, and 2.5 mm, respectively, were obtained. The pressed annular sample was placed in a heat-treatment furnace, heated to the specified temperature (773 K) in an Ar atmosphere, then kept for 1 h in the furnace. After cooling in the furnace, ferrosilicon magnetic cores were obtained.
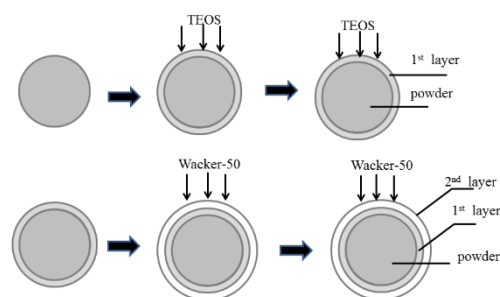
Figure 1. Schematic showing the design of the inorganic/organic double-layer coating.

2.3. Structure and Performance Test

The surface morphologies of the powders before and after coating with insulation and the section morphologies of the sectioned samples were observed using scanning electron microscopy (SEM) (JEOL JXA-8100 (Spatial resolution 3 nm), JEOL, Tokyo, Japan). The phase composition of the powder samples was detected by an X-ray diffractometer (Burker D8 advance (Goniometer accuracy:0.0001°; accuracy ≤ 0.02°) with a Cu Kα target; Bruker, Bremen, Germany). The element distributions in the magnetic powder core were analysed using energy-dispersive X-ray spectroscopy (EDS (accuracy between 1% and 5%)).

The hysteresis loops of the raw materials, composite powders, and SiO_2/organosilicone doubly-insulated ferrosilicon alloy powders were measured with a vibrating sample magnetometer (VSM) (Lakeshore JDAW-2000 (maximum sensitivity is 5×10^{-5} emu), Lake Shore Cryotronics, Shanghai, China) over a magnetic field range of 0–20,000 Oe and at room temperature. The resistivity of the ferrosilicon magnetic core samples was analysed using a four-probe resistivity tester (ST2722-SZ (resolution is 0.5%), TOB New Energy, Jiangsu, China). The magnetic properties of ferrosilicon core samples, such as permeability and magnetic loss, were detected by IWATSU B-H analyzer (SY-8219 (measurement accuracy is 0.05), IWATSU, Shenzhen, China) under the following conditions: temperature = 298 K, that is, under room temperature conditions; Impressed magnetic field = 100 mT; Application magnetic field frequency = 10–100 kHz.

3. Results and Discussion

3.1. Microstructure of the Ferrosilicon Alloy Powder and Doubly Insulated Magnetic Cores

The thermal decomposition of ethyl orthosilicate $C_8H_{20}O_4Si$ is very complex and generates a variety of intermediate organic substances such as $(OC_2H_5)_2Si(OH)_2$, $OSi(OC_2H5)_2$ and $O(Si(OC_2H_5)_3)$ [32]. According to the content of Hess's law, the state at the beginning and end of the reaction determines the heat of the reaction, and the pathway of the chemical reaction does not affect the heat of the reaction. Under atmospheric pressure and non-oxidation conditions, ethylene, water, and silica vapour were the last decomposition substances of $C_8H_{20}O_4Si$. This reaction has the following chemical formula:

$$C_8H_{20}O_4Si(g) \xrightarrow{\Delta} SiO_2(s) + 4C_2H_4(g) + 2H_2O(g)$$
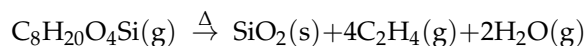
The SEM micrographs in Figure 2 show the microscopic morphologies of the original powder, the Fe-6.5 wt.%Si alloy powder following in situ deposition of the fluidised vapour phase and the double-coated powder. The raw material of the alloy powder (Figure 2a) is uniformly spherical with an approximate particle size of 65 μm. The lines on the powder surface result from atomisation. The alloy powder (Figure 2b) retains its basic shape and size after in situ deposition in the fluidised vapour phase. A dense coating with a rough surface is deposited on the surface. Local magnification reveals a shallower surface-grain concavity of the powder than of the original powder, which is attributable to the filling. Multi-layer accumulation of the filling constitutes a dense coating layer. Figure 2c shows a thin, double-coated alloy powder that has a near-transparent film.
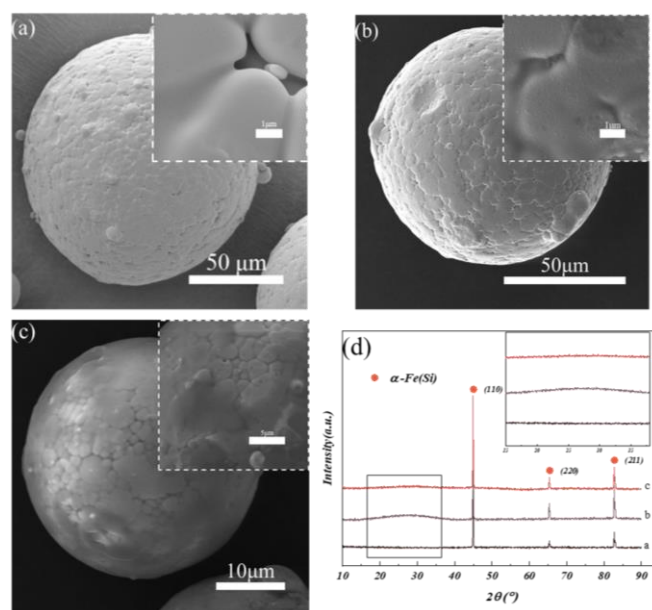
Figure 2. SEM micrographs of (**a**) the raw material, (**b**) the composite powder, and (**c**) the SiO$_2$/organosilicone double-insulated ferrosilicon alloy powder; (**d**) XRD patterns of the powders.

Figure 2d shows the XRD patterns of the original powder, the fluidised deposited powder, and the double-coated particles. All samples display strong diffraction peaks at $2\theta = 44.88°$, $65.12°$ and $82.68°$, corresponding to the (110), (200), and (211) crystal planes of α-Fe(Si), respectively. The peaks obtained by X 'Pert Highscore are consistent with the standard PDF card ICDD09-065-9130. In Figure 2d, the XRD pattern of SiO$_2$-coated powder was compared with the original powder pattern. Apart from the three diffraction peaks of the α-Fe(Si) phase, an extremely obvious broad amorphous 'steamed dough peak' is centred at $2\theta = 25°$. Similar to experimental results reported elsewhere [33,34], this peak is assigned to the amorphous SiO$_2$ phase. However, after recoating with the insulating agent resin, the 'steamed bun peak' is attenuated without shifting its position. Combining this result with the SEM atlas, presumably, an insulating film covers the surface of the powder, this thin film masks the amorphous SiO$_2$ phase, allowing the amorphous peak to remain undetected. It was concluded that composite powders of Fe-6.5 wt.%Si/SiO$_2$ with a core-shell structure were successfully synthesized through the in situ deposition of the original powder fluidised vapour phase. After treatment with the insulating agent, the surface was coated with a resin layer to form an organic–inorganic double-layered insulated magnetic core.

Table 1 lists the elemental surface compositions of three alloy powders, determined by EDS. Fe and Si are the only elements found on the raw material's surface with mass percentages of 94.77 and 6.23 wt.%, respectively, close to the nominal raw-material ratio. In addition, Fe-6.5.wt.%Si alloy powder exhibits O, Fe, and Si on its surface after in situ deposition in the fluidised vapour phase, along with C after treatment with the insulating agent. The C is carried in by the wacker-50 resin component, which attaches to the alloy-powder surface. The double coating reduces the Fe content from 94.77 wt.% to 82.6 wt.% and then to 50.6 wt.% while the Si and O contents increase. After double coating, the average atomic ratio of Si to O on the surface of the alloy powder is about 1:2.

To verify that the double-coated powder pressed core is not destroyed by pressure under a pressing force of 1500 MPa, the magnetic core was broken into small pieces and then inlaid by the hot insert process. After grinding and polishing treatment, the cross-sections were observed under the electron microscope together with local linear scanning and EDS element analysis. The results are shown in Figure 3.

Table 1. Surface compositions of the raw material, the composite powder, and the SiO_2/organosilicone double-insulated coated ferrosilicon alloy powder.

Element	Fe-6.5 wt.%Si		Fe-6.5 wt.%Si/SiO$_2$		Double Coating	
	wt.%	**at.%**	**wt.%**	**at%**	**wt.%**	**at.%**
Fe	94.77	87.68	82.68	63.72	50.6	51.3
Si	6.23	13.32	8.89	13.63	12.1	8.69
O	-	-	8.43	22.65	13.3	20.16
C	-	-	-	-	24	19.85
total	100	-	100	-	100	-
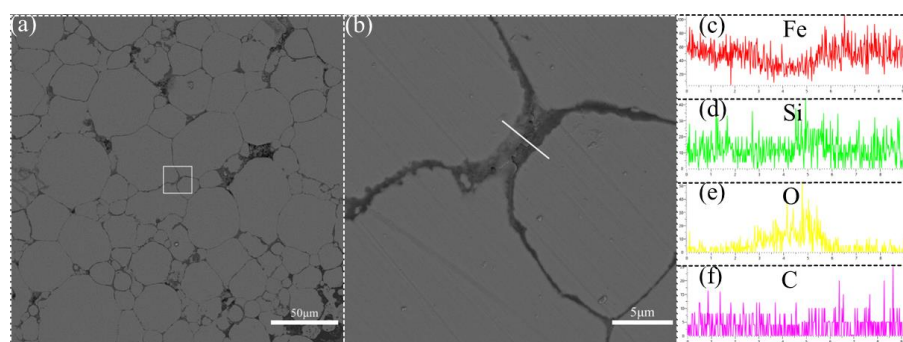
Figure 3. (**a**,**b**) SEM micrographs and (**c**–**f**) line scanning results of the ferrosilicon magnetic core coated with SiO_2/silicone resin double insulation.

In a cross-sectional SEM image of a double-layered composite core (Figure 3a), grayish-white areas are separated by greyish–black areas and the iron core is dense with no gaps. The magnified image in Figure 3b shows that the insulation layer between the powders is complete, continuous, and uniform [33]. The SiO_2 layer produced by the fluidised vapour in situ deposition process is also continuous and uniform, indicating that it was not destroyed. The linear scanning results in this region are illustrated in Figure 3c–f. The Fe element is mainly distributed at both ends of the greyish–black region. At the interface of the particles in the Fe-6.5 wt.%Si composite magnetic particle core, the Fe content decreases while the Si and O contents are far increased above those of the single-coated sample. This finding shows that the Fe-Si core in the composite is well separated by the SiO_2 shell between the particles and thus insulated from each other. Elemental C from the insulating resin is also present. These insulation layers will help improve resistivity, which in turn will reduce eddy current losses.

3.2. Influence of Organic Resin Content on the Properties of the Doubly Coated Ferrosilicon Magnetic Core

Figure 4 shows the SEM results of the powders combined with different amounts of insulating resin. Different from powders that are only coated with SiO_2 (Figure 4a), the powder coated with insulating resin shows a gel-like layer on its surface (Figure 4b–d). Intuitively, increasing the resin content gradually increases the coverage area of the organic insulation layer on the powder surface. As seen in Figure 4b, the 1.1-wt.% resin is insufficient to cover the powder and many parts of the surface remain bare. However, the 1.5 wt.% resin forms a complete and uniform organic coating on the powder surface (Figure 4c) and no small particles are adsorbed on the organic insulation layer. When the added amount reaches 2.0 wt.%, the insulation layer thickens and small particles are easily agglomerated, probably because a large amount of insulating resin promotes adhesion between the powders, hindering dispersion and distribution of the powders and thus affecting the arrangement and combination during powder pressing.
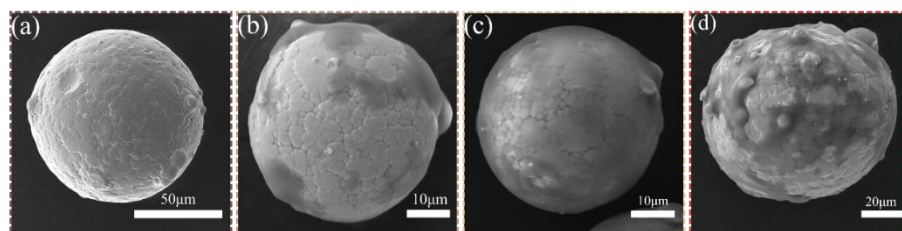
Figure 4. SEM atlas of ferrosilicon alloy powder coated with SiO_2/silicone resin double insulation containing different amounts of silicone resin: (**a**) 0.5, (**b**) 1.0, (**c**) 1.5, and (**d**) 2.0 wt.%.

VSM was used to analyze the hysteresis loop of powder to study the performance of Fe-6.5 wt.%Si/SiO_2 composite powder after the addition of insulating resin.

All powders exhibit the typical soft-magnetic characteristics of high permeability and low coercivity (Figure 5a). The saturation magnetization strength of the powder coated only with SiO_2 was 202.7 emu/g. After coating with 1.0, 1.5, and 2.0 wt.% insulating resin, the M_s values reduce to 195.2, 187.5, and 183.9 emu/g, respectively. When the insulating resin is added to the composite powder, it increases the nonmagnetic phase content, which dilutes the magnetic properties of the composite powder; accordingly, as the resin content increases, the saturation magnetic strength of the powder gradually decreases. In contrast, the coercivity of double-coated powders is similar to that of single-layer coated SiO_2 powders (Figure 5b) because coercivity is an inherent property of the material. The magnetic domain in each core particle is unaffected by both the SiO_2-deposited layer and the silicone-insulating layer [35], so the coercivity of all particles is almost constant.
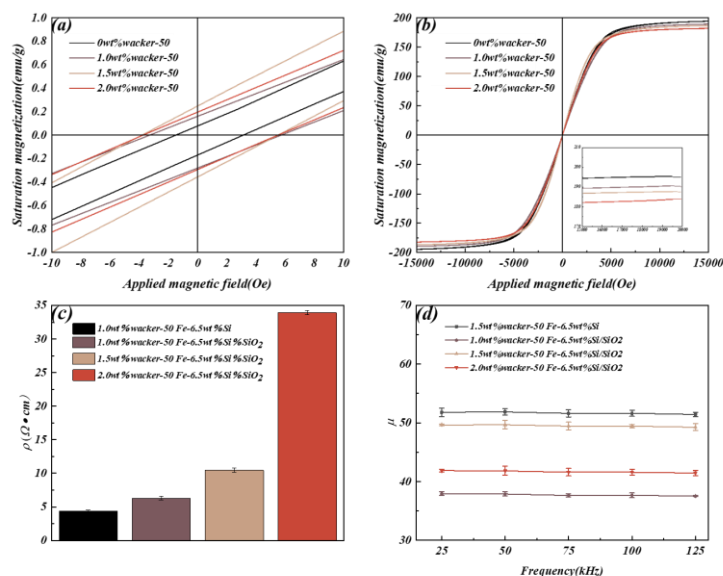
Figure 5. (**a**) Hysteresis loops of double-layer coated cores with different resin content, (**b**) coercivity diagrams, (**c**) resistivity, and (**d**) magnetic permeability.

Eddy current heat causes eddy current losses, which are inversely proportional to resistivity. Therefore, high resistivity is a desired property of a soft magnetic material. A metal soft magnetic core's resistivity depends on the magnetic powder it uses, the type of insulation coating, and the proportion of air gap in the core.

The bar chart in Figure 5c compares the surface resistivities of annealed Fe-6.5 wt.%Si magnetic powder cores with different amounts of insulation coating. One of the samples with no SiO_2 insulating layer exhibits the lowest resistivity (4.4 cells/cm). As the amounts of insulating resin increases from 1 wt.% to 1.5 wt.% to 2 wt.%, the resistivities of the magnetic particle core gradually increase to 6.3, 10.5, and 33.9 Ω·cm respectively. A reduction in electron mobility after coating the magnetic powder core with SiO_2 insulating layer can

explain this trend. Consequently, the resistivity of the magnetic powder core improves after double-coating. However, when the amount of insulation coating liquid is small, the insulation layer on the ferrosilicon alloy powder particles is incompletely coated and the ferrosilicon magnetic particles are in direct contact, so the surface resistivity of the core is small. As the amount of insulation-coating liquid increases, a complete insulation-coating layer is gradually formed on the powder particles and the thickness of this layer also gradually increases. Correspondingly, its surface resistivity also increases.

Figure 5d depicts the permeabilities of the magnetic particle cores with different amounts of insulating resin, obtained at 100 mT and 50 kHz.

As evidenced in the figure, the effective permeabilities of magnetic cores coated with different amounts of insulating resin change little with frequency, indicating that the magnetic cores coated with double-layer resins maintain their stable high-frequency characteristics over a wide frequency range. When the original powder is coated with insulating resin alone, the effective permeability is 52. In the doubly coated Fe-6.5 wt.%Si/SiO_2 magnetic powder cores, the effective permeabilities are 37, 49, and 42 at resin contents of 1.0, 1.5, and 2.0 wt.%, respectively. This behaviour reflects the fact that permeability is related not only to the density of the magnetic core but also to the amount of magnetic material per unit volume. The powder particles treated by the fluidised in-situ deposition process are covered with a SiO_2 insulating layer and have much higher magnetic-substance contents per unit volume than powder particles coated only with insulating resin; therefore, their permeability is reduced.

As more insulating resin is added, the effective permeability first increases and then decreases. The effective permeability is maximized (at 49) in the core coated with 1.5 wt.% resin because this coating improves the arrangement of the inter-powders. At 1.1 wt.%, the organic insulating layer on the outer surface of the powder is non-uniformly and incompletely coated, the bonding is ineffective, which cannot play the role of insulation between powders (see the SEM images in Figure 4). A number of pores between the powders appear in the magnetic powder core, decreasing the density under a certain compression pressure, hence, deteriorating the permeability. However, when the amount of insulating organic resin increases to 2.0 wt.%, the organic insulating layer becomes thicker and the content of non-magnetic substances increases. Thus, an excessive amount of insulating agent increases the unevenness of the powder arrangement and dispersion. The large particles are then easily agglomerated before pressing, increasing the porosity of the magnetic core while decreasing the density. The permeability then drops. After adding 1.5 wt.% insulating organic resin-coated powder, the amount of non-magnetic substances was appropriate and the powder adhesion and uniformity of particle dispersion improved, thus increasing the density and permeability of the magnetic powder core.

Figure 6a shows the frequency dependences of the magnetic core losses in raw material and single-layer coated powder with different wacker dosages. Panels (b) and (c) of Figure 6 plot the eddy current losses and hysteresis losses, respectively.

As demonstrated in Figure 6a, the core losses of the magnetic powders pressed with powders containing different amounts of insulating resins increase with frequency. At the same test frequency, the total loss is much lower in the double-coated magnetic core than in its single-coated counterpart (905 mW/cm^3 versus 1215 mW/cm^3 at 100 mT and 50 kHz). This result can be analysed by considering the composition of the loss. At a pressing force of 1500 MPa, the SiO_2 insulation layer completely covers the magnetic particle core, resulting in low eddy current losses. The complete layer effectively blocks the eddy current leakage. Further, the hysteresis loss mainly depends on the magnetostrictive coefficient, magnetic-crystal anisotropy constant, internal stress, and phase transitions in the alloy. In this experiment, the magnetic cores were annealed at constant annealing temperature and the alloys followed a consistent transformation law, so the loss cannot be attributed to transformations in the alloy. In Fe–Si systems, increasing the percentage of Si atoms reduces both the magnetostrictive coefficient and the magnetic-crystal anisotropy constant.

Therefore, introducing the SiO_2 insulation layer increases the percentage of Si atoms in the sample, thus reducing the hysteresis loss.
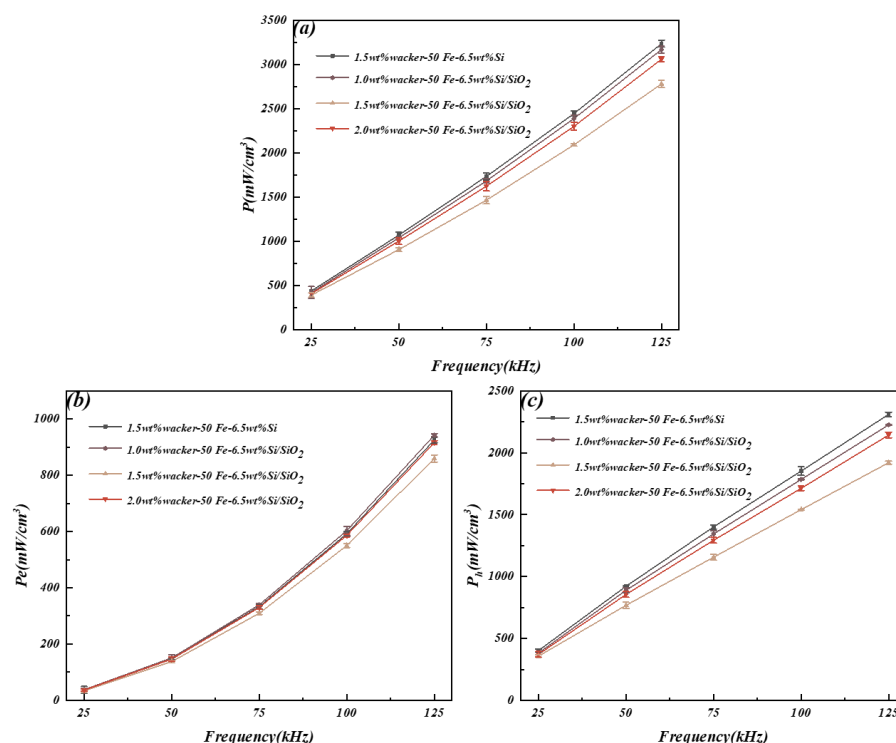
Figure 6. Frequency dependencies of (**a**) total losses, (**b**) eddy current losses and (**c**) hysteresis loss is in a double-layer coated core with different insulating resins.

As the amount of organic insulating resin increases in the double-coated powders, the total loss of the composite magnetic core first decreases and then increases. At resin contents of 1.0, 1.5, and 2.0 wt.%, the magnetic core losses are 1039, 905, and 1001 mW/cm^3, respectively, at 100 mT and 50 kHz. As evidenced in Figure 6b,c, the eddy current losses and hysteresis losses are both minimised at 1.5 wt.% because the insulating resin is effectively coated on the powder surface. Between 1.0 and 1.5 wt.%, the resin is effectively filled between the micron-sized powder particles. As the composite magnetic core contains very few pores, it has a small total loss. When the amount of wacker resin is further increased to 2.0 wt.%, the loss of the composite magnetic core again increases because the large-scale agglomeration of micron powder prevents the rearrangement of powder particles during the pressing process. Therefore, the composite magnetic core develops more pores, and the coercivity increases, leading to an increase in hysteresis loss. Eddy current loss is composed of losses within and between particles, resistivity and particle size are the main factors affecting powder properties. Increasing the resistivity can reduce the eddy current between particles. Judging from the slightly increased eddy current loss in the composite magnetic core, the decrease of eddy current loss within particles is greater than that of vortex loss between particles.

3.3. Influence of Moulding Pressure on the Structure and Properties of the Ferrosilicon Magnetic Core

Continue to increase the properties of the core without damaging the SiO_2/silicone resin double insulation layer, a ferrosilicon magnetic core containing 1.5 wt.% silicone resin was prepared at a constant annealing temperature (773 K) and different pressures (1200, 1300, 1400, 1500, and 1600 MPa).

Figure 7a shows the influence of compression pressure on the permeability of the Fe-6.5 wt.%Si/SiO_2 composite magnetic cores. Within the frequency range of 25–150 kHz,

the permeabilities of the cores remain stable under a given pressure. Under different pressures at 50 kHz, the permeabilities of the composite magnetic core increase as follows: 45.1 (1200 MPa), 47.7 (1300 MPa), 48.3 (1400 MPa), 49.6 (1500 MPa) and 53.4 (1600 MPa). The densities of these composite magnetic cores were also measured and plotted in Figure 7b. High compression pressure increases the density by promoting the rearrangement of the powder particles during the pressing process. The tiny Fe-6.5 wt.%Si particles fully occupy the spaces between the large powder particles, reducing the number of pores and thus increasing the density. Therefore, an appropriate setting of the pressing pressure can effectively increase the density of the core, which in turn increases the permeability of the core.
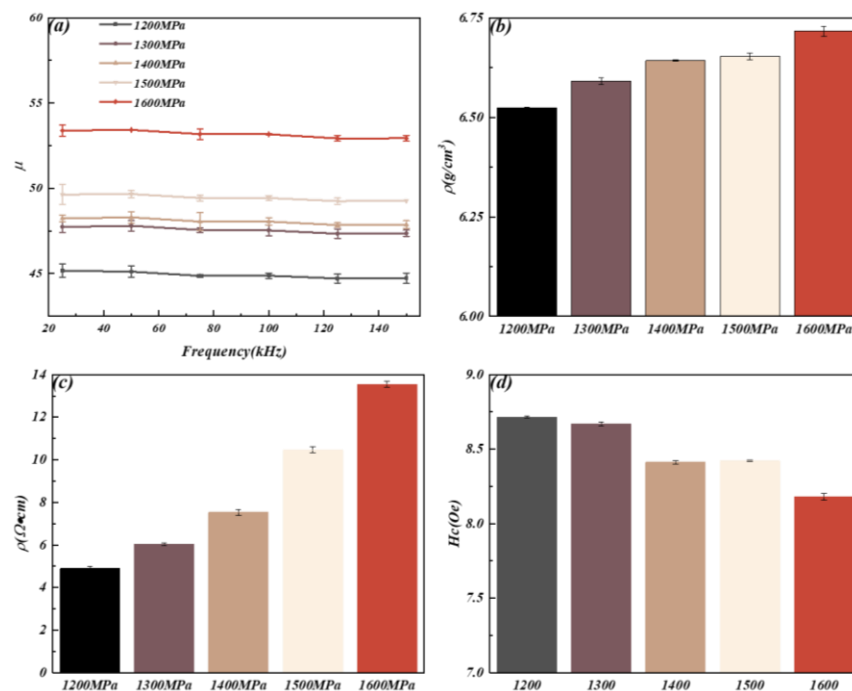
Figure 7. (**a**) Permeabilities, (**b**) densities, (**c**) resistivities, and (**d**) coercivities of the ferrosilicon magnetic core under different compression pressures.

As shown in Figure 7c, the resistivity of the Fe-6.5 wt.%Si/SiO$_2$ composite magnetic core gradually increases from 4.8 to 13.5 Ω·cm as the compression pressure increases. This occurs because under high compression pressures, as a result of shear forces, the partially agglomerated particles are depolymerised and separated. The resistivity of the magnetic core is then increased. Furthermore, the coercivity of the composite magnetic core decreases from 8.7 Oe at 1200 MPa to 8.1 Oe at 1600 MP (Figure 7d) because the promoted rearrangement of the powder particles under compression decreases the quantity of pores in the composite magnetic core. The domain-wall movement is less obstructed and the magnetic core density is increased, with a concomitant reduction in coercivity.

Figure 8 plots the effect of compression pressure on the core loss in the Fe-6.5 wt.%Si/SiO$_2$ ferrosilicon magnetic core. The magnetic core loss increases as the frequency increases from 25 to 150 kHz. As shown in the loss- distribution bar chart in the upper left corner of Figure 8a, the total loss of the ferrosilicon magnetic core decreases with increasing compression pressure. At 100 mT and 50 kHz, the total loss decreases from 933.3 mW/cm^3 at 1200 MPa to 881.5 mW/cm^3 at 1600 MPa. To explore how the compression pressure influences the loss of the ferrosilicon magnetic core, the losses in the magnetic core were separated. Increasing the compression pressure hardly changes the eddy current loss at any frequency (Figure 8b). In contrast, the hysteresis loss of the magnetic core is affected by compression pressure and is minimised under 1600 MPa at each frequency (Figure 8c). The loss of the medium frequency core is mainly hysteresis loss, the eddy current loss

accounts for a small proportion. Combined with the coercivity and resistivity analyses in Figure 7, one finds that increasing the compressing pressure increases the resistivity inside the magnetic core but little affects the eddy current loss. Moreover, increasing the density reduces the coercivity, thereby reducing hysteresis loss inside the magnetic core. Accordingly, the total loss of the magnetic core is affected.
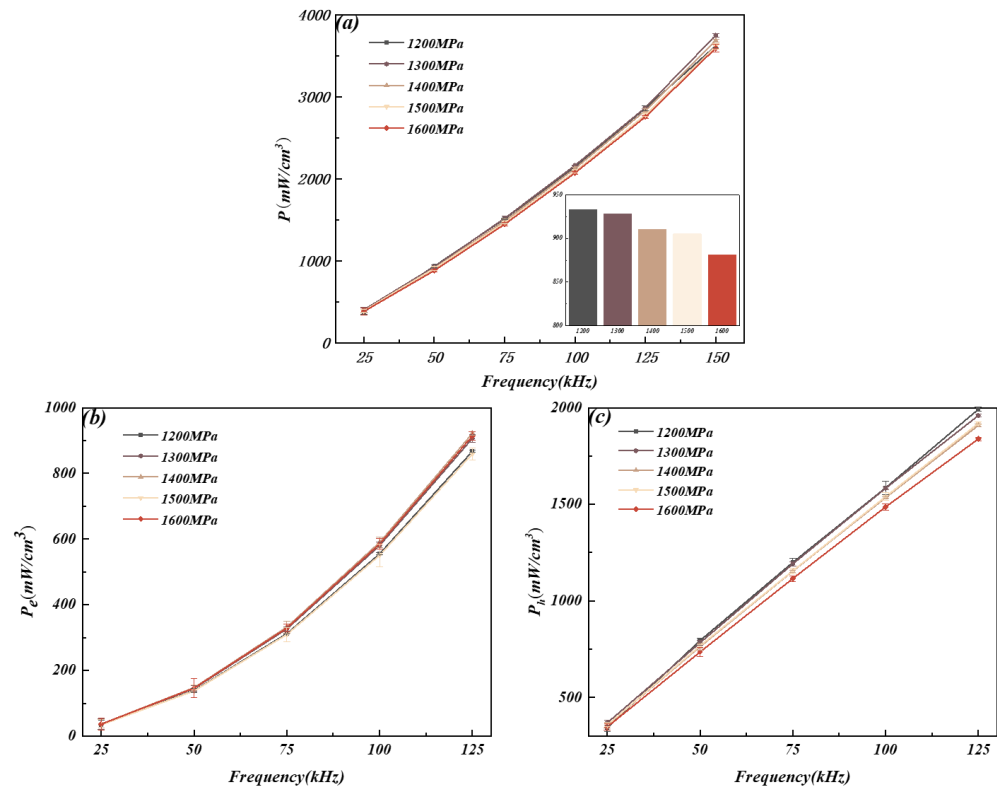
Figure 8. (**a**) Total losses, (**b**) eddy current losses, and (**c**) hysteresis losses of ferrosilicon magnetic cores formed under different compression pressures.

4. Conclusions

The main conclusions are summarised below:

1. In ferrosilicon magnetic cores doubly coated with SiO_2/silicone resin insulation, increasing the silicone resin content of the insulation coating gradually thickened the coating, decreased the saturation magnetic-induction intensity of the ferrosilicon magnetic core, and increased and then decreased the effective permeability and density of the ferrosilicon magnetic core. At an organic resin content of 1.5 wt.%, the insulation coating on the powder was optimised, the magnetic core loss was lowest and the permeability was highest.

2. Increasing the forming pressure improves the performance of the magnetic core. As the pressure increases, the permeability and loss of the magnetic core gradually increased and decreased, respectively, provided that the double cladding layer remained undamaged.

3. At a silicone resin content of 1.5 wt.%, the magnetic properties were optimised by preparing the magnetic cores at 1500 MPa after heat treatment at 773 K. The saturation magnetisation was 187.5 emu/g and the resistivity and permeability were as high as 10.5 $\Omega\cdot$cm and 49.6, respectively, at 100 mT and 50 kHz. The total loss was 905 mW/cm^3.

References

1. Vijayakumar, K.; Thiagarajan, Y.; Rajendirakumar, R.; Joseph Basanth, A.; Karthikeyan, R.; Kannan, S. Development of an iron powder metallurgy soft magnetic composite core switched reluctance motor. *Mater. Today Proc.* **2021**, *41*, 1195–1201. [CrossRef]
2. Talaat, A.; Suraj, M.V.; Byerly, K.; Wang, A.; Wang, Y.; Lee, J.K.; Ohodnicki, P.R. Review on soft magnetic metal and inorganic oxide nanocomposites for power applications. *J. Alloys Compd.* **2021**, *870*, 159500. [CrossRef]
3. Shokrollahi, H.; Janghorban, K. Soft magnetic composite materials (SMCs). *J. Mater. Process. Technol.* **2007**, *189*, 1–12. [CrossRef]
4. Svensson, L.; Frogner, K.; Jeppsson, P.; Cedell, T.; Andersson, M. Soft magnetic moldable composites: Properties and applications. *J. Magn. Magn. Mater.* **2012**, *324*, 2717–2722. [CrossRef]
5. Ouyang, G.; Chen, X.; Liang, Y.; Macziewski, C.; Cui, J. Review of Fe-6.5 wt%Si high silicon steel—A promising soft magnetic material for sub-kHz application. *J. Magn. Magn. Mater.* **2019**, *481*, 234–250. [CrossRef]
6. Li, K.; Cheng, D.; Yu, H.; Liu, Z. Process optimization and magnetic properties of soft magnetic composite cores based on phosphated and mixed resin coated Fe powders. *J. Magn. Magn. Mater.* **2020**, *501*, 166455. [CrossRef]
7. Meng, B.; Yang, B.; Zhang, X.; Zhou, B.; Li, X.; Yu, R. Combinatorial surface coating and greatly-improved soft magnetic performance of Fe/Fe_3O_4/resin composites. *Mater. Chem. Phys.* **2020**, *242*, 122478. [CrossRef]
8. Birčáková, Z.; Füzer, J.; Kollár, P.; Streckova, M.; Szabó, J.; Bureš, R.; Fáberová, M. Magnetic properties of Fe-based soft magnetic composite with insulation coating by resin bonded Ni-Zn ferrite nanofibres. *J. Magn. Magn. Mater.* **2019**, *485*, 1–7. [CrossRef]
9. Choi, K.D.; Lee, S.Y.; Hwang, J.S.; Yang, S.; Huh, J.Y.; Yi, K.W.; Byun, J.Y. Magnetic properties of Fe soft magnetic composites with a double-insulating layer comprising Fe_3O_4 and silicone resin. *J. Alloys Compd.* **2023**, *936*, 168255. [CrossRef]
10. Taghvaei, A.H.; Shokrollahi, H.; Ebrahimi, A.; Janghorban, K. Soft magnetic composites of iron-phenolic and the influence of silane coupling agent on the magnetic properties. *Mater. Chem. Phys.* **2009**, *116*, 247–253. [CrossRef]
11. Wu, S.; Sun, A.; Zhai, F.; Wang, J.; Zhang, Q.; Xu, W.; Logan, P.; Volinsky, A.A. Annealing effects on magnetic properties of silicone-coated iron-based soft magnetic composites. *J. Magn. Magn. Mater.* **2012**, *324*, 818–822. [CrossRef]
12. Jin, X.; Li, T.; Jia, Z.; Shi, H.; Xue, D. Over 100 MHz cut-off frequency mechanism of Fe-Si soft magnetic composites. *J. Magn. Magn. Mater.* **2022**, *556*, 169366. [CrossRef]
13. Zhang, Y.; Dong, Y.; Zhou, B.; Chi, Q.; Chang, L.; Gong, M.; Huang, J.; Pan, Y.; He, A.; Li, J.; et al. Poly-para-xylylene enhanced Fe-based amorphous powder cores with improved soft magnetic properties via chemical vapor deposition. *Mater. Des.* **2020**, *191*, 108650. [CrossRef]
14. Chen, Y.; Zhang, L.; Sun, H.; Chen, F.; Zhang, P.; Qu, X.; Fan, E. Enhanced magnetic properties of iron-based soft magnetic composites with phosphate-polyimide insulating layer. *J. Alloys Compd.* **2020**, *813*, 152205. [CrossRef]
15. Zhou, B.; Dong, Y.; Liu, L.; Chang, L.; Bi, F.; Wang, X. Enhanced soft magnetic properties of the Fe-based amorphous powder cores with novel TiO2 insulation coating layer. *J. Magn. Magn. Mater.* **2019**, *474*, 1–8. [CrossRef]
16. Hsiang, H.-I.; Fan, L.-F.; Hung, J.-J. Phosphoric acid addition effect on the microstructure and magnetic properties of iron-based soft magnetic composites. *J. Magn. Magn. Mater.* **2018**, *447*, 1–8. [CrossRef]
17. Ishizaki, T.; Nakano, H.; Tajima, S.; Takahashi, N. Improving Powder Magnetic Core Properties via Application of Thin, Insulating Silica-Nanosheet Layers on Iron Powder Particles. *Nanomaterials* **2017**, *7*, 1. [CrossRef]
18. Geng, K.; Xie, Y.; Xu, L.; Yan, B. Structure and magnetic properties of ZrO_2-coated Fe powders and Fe/ZrO_2 soft magnetic composites. *Adv. Powder Technol.* **2017**, *28*, 2015–2022. [CrossRef]
19. Peng, Y.; Yi, Y.; Li, L.; Yi, J.; Nie, J.; Bao, C. Iron-based soft magnetic composites with Al_2O_3 insulation coating produced using sol–gel method. *Mater. Des.* **2016**, *109*, 390–395. [CrossRef]
20. Qiu, Y.; Wang, R.; He, Y.; Kong, H.; Li, S.; Wu, Z. Effects of axial pressure on the evolution of core–shell heterogeneous structures and magnetic properties of Fe–Si soft magnetic powder cores during hot-press sintering. *RSC Adv.* **2022**, *12*, 19875–19884. [CrossRef]

21. Wu, Z.; Liao, X.; Wang, R.; Gao, Z.; Xu, L.; Wang, J. Development of quantitative parameter–property relationship and technology parameter choosing software of Fe(Si)–SiO$_2$ soft ferromagnetic composites. *J. Mater. Res. Technol.* **2022**, *17*, 441–451. [CrossRef]

22. Pozo López, G.; Condó, A.M.; Urreta, S.E.; Silvetti, S.P. Synthesis of Fe/SiO$_2$ and iron oxides/SiO$_2$ nanocomposites by long-term ball milling. *Mater. Res. Bull.* **2014**, *49*, 237–244. [CrossRef]

23. Chen, H.; Deng, C.; Zhang, X. Synthesis of Fe$_3$O$_4$@SiO$_2$@PMMA Core–Shell–Shell Magnetic Microspheres for Highly Efficient Enrichment of Peptides and Proteins for MALDI-ToF MS Analysis. *Angew. Chem. Int. Ed.* **2010**, *49*, 607–611. [CrossRef] [PubMed]

24. Zheng, J.; Zheng, D.; Qiao, L.; Ying, Y.; Tang, Y.; Cai, W.; Li, W.; Yu, J.; Li, J.; Che, S. High permeability and low core loss Fe-based soft magnetic composites with Co-Ba composite ferrite insulation layer obtained by sol-gel method. *J. Alloys Compd.* **2022**, *893*, 162107. [CrossRef]

25. Chen, J.; Guo, H.; Zhong, X.; Fu, J.; Huang, S.; Xie, X.; Li, L. Microstructural and magnetic properties of core-shell FeSiAl composites with Ni$_{0.4}$Zn$_{0.45}$Co$_{0.15}$Fe$_2$O$_4$ layer by sol-gel method. *J. Magn. Magn. Mater.* **2021**, *529*, 167774. [CrossRef]

26. Ma, L.; Liu, Y.; Li, J.; Jin, N.; Li, C.; Zhou, X.; Ma, J. A new way for lead–boron resin composite modification: SiO$_2$ coated lead powders by a sol–gel method. *RSC Adv.* **2019**, *9*, 30752–30759. [CrossRef]

27. Wu, S.; Sun, A.; Lu, Z.; Cheng, C.; Gao, X. Magnetic properties of iron-based soft magnetic composites with SiO$_2$ coating obtained by reverse microemulsion method. *J. Magn. Magn. Mater.* **2015**, *381*, 451–456. [CrossRef]

28. Liu, L.; Liao, X.W.; Jia, J.X.; Kong, H.; Fan, X.A.; Wu, Z.Y.; Wang, X.S. Temperature-controlled conversion from Fe–Si particles to integrated Fe–Si/SiO2 core–shell structure particles during fluidised bed chemical vapour deposition. *Ceram. Int.* **2020**, *46*, 3059–3065. [CrossRef]

29. Wu, Z.Y.; Jiang, Z.; Fan, X.A.; Zhou, L.J.; Wang, W.L.; Xu, K. Facile synthesis of Fe-6.5wt%Si/SiO$_2$ soft magnetic composites as an efficient soft magnetic composite material at medium and high frequencies. *J. Alloys Compd.* **2018**, *742*, 90–98. [CrossRef]

30. Pu, H.; Jiang, F.; Wang, Y.; Yan, B. Soft magnetic composite particles of reduced iron coated with poly(p-xylylene) via chemical vapor deposition polymerization. *Colloids Surf. A: Physicochem. Eng. Asp.* **2010**, *361*, 62–65. [CrossRef]

31. Huang, H.; Wang, R.; Chen, R.; Li, M.; Hou, Q.; Wu, Z.; Huang, Z. Understanding the growth mechanism of SiO$_2$ on the surface of FeSi clusters: An MD and DFT simulation study. *J. Sol-Gel Sci. Technol.* **2022**, *102*, 335–342. [CrossRef]

32. Coltrin, M.E.; Ho, P.; Moffat, H.K.; Buss, R.J. Chemical kinetics in chemical vapor deposition: Growth of silicon dioxide from tetraethoxysilane (TEOS). *Thin Solid Film.* **2000**, *365*, 251–263. [CrossRef]

33. Fan, X.A.; Wu, Z.Y.; Li, G.Q.; Wang, J.; Xiang, Z.D.; Gan, Z.H. High resistivity and low core loss of intergranular insulated Fe–6.5wt.%Si/SiO$_2$ composite compacts. *Mater. Des.* **2016**, *89*, 1251–1258. [CrossRef]

34. Zhang, J.; Tu, R.; Goto, T. Densification of SiO$_2$–cBN composites by using Ni nanoparticle and SiO$_2$ nanolayer coated cBN powder. *Ceram. Int.* **2012**, *38*, 4961–4966. [CrossRef]

35. Geng, K.; Xie, Y.; Yan, L.; Yan, B. Fe-Si/ZrO$_2$ composites with core-shell structure and excellent magnetic properties prepared by mechanical milling and spark plasma sintering. *J. Alloys Compd.* **2017**, *718*, 53–62. [CrossRef]